AJNR

MR Imaging and Proton Spectroscopy of Neuronal Injury in Late-Onset G $_{M2}$ Gangliosidosis

Matilde Inglese, Annette O. Nusbaum, Gregory M. Pastores, John Gianutsos, Edwin H. Kolodny and Oded Gonen

AJNR Am J Neuroradiol 2005, 26 (8) 2037-2042
http://www.ajnr.org/content/26/8/2037

MR Imaging and Proton Spectroscopy of Neuronal Injury in Late-Onset G_{M2} Gangliosidosis

Matilde Inglese, Annette O. Nusbaum, Gregory M. Pastores, John Gianutsos, Edwin H. Kolodny, and Oded Gonen

BACKGROUND AND PURPOSE: **Despite the ubiquity of G_{M2} gangliosides accumulation in patients with late-onset G_{M2} gangliosidosis ($G_{M2}G$), the only clinical MR imaging–apparent brain abnormality is profound cerebellar atrophy. The goal of this study was to detect the presence and assess the extent of neuroaxonal injury in the normal-appearing gray and white matter (NAGM and NAWM) of these patients.**

METHODS: **During a single imaging session, 9 patients with late-onset $G_{M2}G$ and 8 age-matched normal volunteers underwent the following protocol: (1) T1- and T2-weighted and fluid-attenuated inversion recovery MR images, as well as (2) multivoxel proton MR spectroscopy (^{1}H-MR spectroscopy) to quantify the distribution of the N-acetylaspartate (NAA), creatine (Cr), and choline (Cho), were obtained.**

RESULTS: **The patients' NAA levels in the thalamus (6.5 ± 1.9 mmol/L) and NAWM (5.8 ± 2.1 mmol/L) were ~40% lower than the controls' ($P = .003$ and $P = .005$), whereas the Cr and Cho reductions (~30% and ~26%) did not reach significance (P values of .06–.1). All cerebellar metabolites, especially NAA and Cr, were much (30%–90%) lower in the patients, which reflects the atrophy.**

CONCLUSION: **In late-onset $G_{M2}G$, NAA decreases are detectable in NAGM and NAWM even absent morphologic (MR imaging) abnormalities. Because the accumulation of G_{M2} gangliosides can be reduced pharmacologically, ^{1}H-MR spectroscopy might be a sensitive and specific for detecting and quantifying neuroaxonal injury and monitoring response to emerging treatments.**

Late-onset G_{M2} gangliosidosis ($G_{M2}G$) is a rare lysosomal storage disorder resulting from mutations of the α subunit of the lysosomal enzyme β-hexosaminidase A (βHex A), which catalyzes the degradation of G_{M2} ganglioside (1). The ensuing progressive accumulation of G_{M2} gangliosides within neurons has been associated with ectopic dendritogenesis, meganeurite formation, and apoptosis (2). βHex A gene mutations, most prevalent among Jews of Ashkenazi ancestry, may lead to either an infantile or the later-onset clinical subtypes, both of which are inherited autosomal recessive traits (3). Although the "classic" infantile form (Tay-Sachs disease) is a rapidly progressive neurodegeneration leading to death in the first few years of life, in the less common, late-onset form, the disease is delayed until childhood or early adulthood (4). This subtype exhibits a clinical picture characterized by dysarthria, dysmetria, ataxia, and various other signs of cerebellar and anterior motor neuron involvement (5). Most patients also suffer from psychiatric symptoms—eg, psychotic episodes and bipolar disorder (6). Genetic analysis reveals that most late-onset $G_{M2}G$ patients are compound heterozygotes, with one severe and one mild gene defect (usually the G269S mutation) associated with residual enzyme activity (1).

Unlike the infantile form, in late-onset $G_{M2}G$, progressive cerebellar atrophy is the only abnormality on conventional MR imaging (compare Fig 1*A*); the supratentorial structures appear completely normal, as shown in Fig 2*A* (7–9). In postmortem examination, however, gangliosides are found not only in cerebellar neurons, but also throughout the neuroaxis, predominantly in deep cerebral nuclei, the hypothalamus, the substantia nigra, and other brain stem nuclei (10).

Received December 3, 2004; accepted after revision February 11, 2005.

From the Departments of Radiology (M.I., A.O.N., O.G.), Neurology (G.M.P., E.H.K.), and Rehabilitation Medicine (J.G.), New York University, New York, NY.

This work was supported by National Institutes of Health grants EB01015, NS051623, NS39135, and NS050520, and by Celltech Group PLC, Berkshire, United Kingdom.

Address correspondence to Matilde Inglese, MD, Department of Radiology, New York University, 650 1st Avenue, 6th Floor, New York, NY 10016.

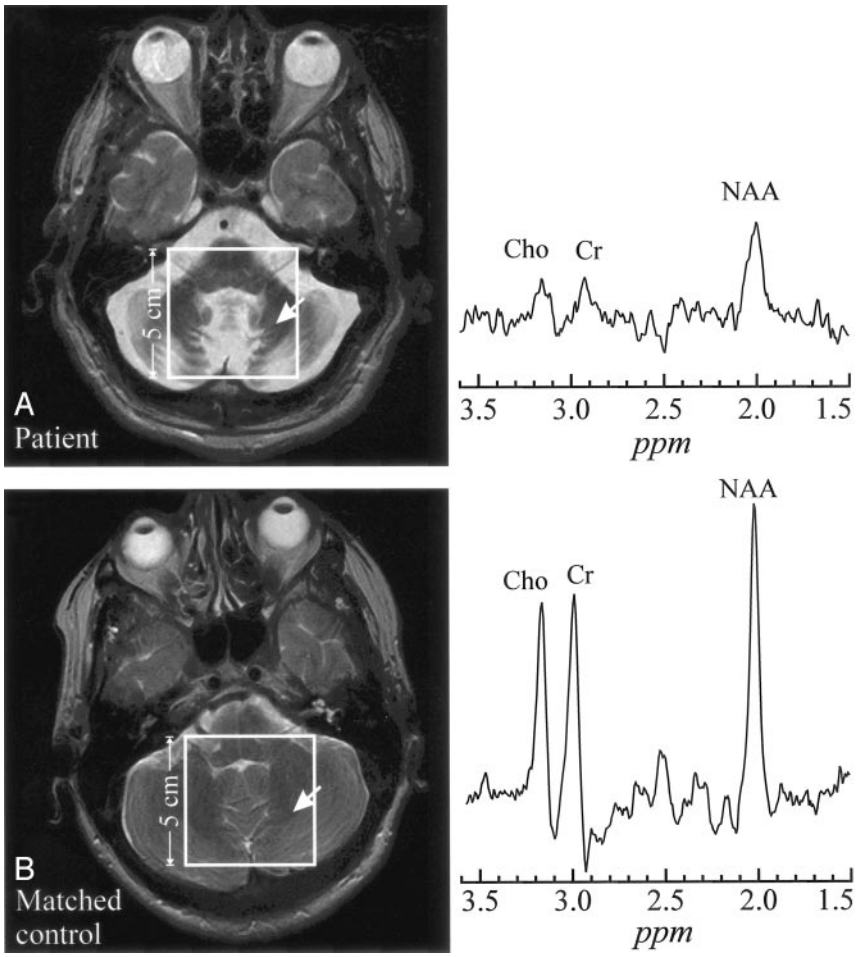

FIG 1. *A, top left,* Axial T2-weighted image from a 54-year-old late-onset $G_{M2}G$ patient superimposed with the 5 × 5 cm^2 VOI. *Right,* ^{1}H spectrum from the cerebellum (*arrow*).

B, bottom left, Corresponding section from a 52-year-old healthy control superimposed with the 5 × 5 cm^2 VOI. *Right,* Arrow indicates analogous region for metabolite comparison. Both spectra are on the same scale. Note the dramatic atrophy of the cerebellar folia and vermis in the patient and consequent lower metabolites levels reflecting larger partial CSF volume contamination.

Proton MR spectroscopy (^{1}H-MR spectroscopy), a noninvasive assay of brain metabolism, has been applied to the study of CNS disorders, including the lysosomal storage diseases (11–14). The main detectable metabolites are (1) N-acetylaspartate (NAA), which is almost exclusively localized in neurons and their processes (11) and whose decrease, even beyond MR imaging abnormalities, has been associated with neuroaxonal injury or loss (15–20); (2) phosphocholine and glycerol phosphocholine (Cho), whose changes reflect membrane turnover; and (3) phosphocreatine and creatine (Cr), which act as reserves for high-energy phosphates in the cytosol of neurons and glial cells (21).

In this report, we compared MR imaging and metabolic characteristics of late-onset $G_{M2}G$ patients with age-matched controls to (1) assess the presence and the extent of neuro/axonal injury in regions of normal-appearing gray and white matter (NAGM and NAWM) and (2) identify potential metabolic markers of the disease and determine their impact on clinical manifestations.

Methods

Human Subjects

Nine late-onset $G_{M2}G$ patients (6 men and 3 women; mean age, 39 years; age range, 20–58 years; 6 patients of Ashkenazi Jewish ancestry) were studied. Their demographic, clinical, and genetic data are compiled in Table 1. All showed different extent of cerebellar involvement. Specifically, 4 had mild, 4 moderate, and one severe tremor; 2 complained of mild, 4 moderate, and 2 severe dysarthria. In addition, 4 patients suffered mild, 4 moderate, and 2 severe weakness, and 4 patients were receiving psychotropic medication for treatment of psychiatric symptoms. Eight age- and sex-matched healthy controls (5 men and 3 women; mean age, 38 years; age range, 21–52 years) underwent the same MR imaging and MR spectroscopy procedures. The study was approved by our local institutional review board, and written informed consent was obtained from all subjects or their guardians.

MR Imaging and MR Spectroscopy

MR imaging and ^{1}H-MR spectroscopy were performed in a 1.5T whole-body imager and standard quadrature head-coil (Siemens, Erlangen, Germany). MR imaging comprised axial T2-weighted (TE/TR, 104/4500 ms; 210 × 210 mm^2 field-of-view [FOV]; 208 × 256 matrix; 90° flip angle [FA)]), axial and sagittal fluid-attenuated inversion recovery (TE/TR/TI, 111/9000/2500 ms; 210 × 210 mm^2 FOV; 256 × 256 matrix; 90° FA), and axial and sagittal T1-weighted (TE/TR, 4/1130 ms; 230 × 230 mm^2 FOV; 512 × 512 matrix; 15° FA) images. All axial sequences imaged 20 5-mm-thick sections.

Multivoxel water-suppressed ^{1}H-MR spectroscopy was performed by using point-resolved spectroscopic sequencing (TR/TE, 1500/144 ms) with 16 × 16 weighted *k*-space phase-encoding over a 16 × 16 cm^2 FOV, leading to effective spatial resolution (voxel size) of 1.5-cm anterioposterior (AP) × 1.5-cm left-right (LR) × 1.5-cm craniocaudal (CC) = 3.4 cm^3. For each subject, a 5-cm AP × 5-cm LR × 1.5-cm CC volume

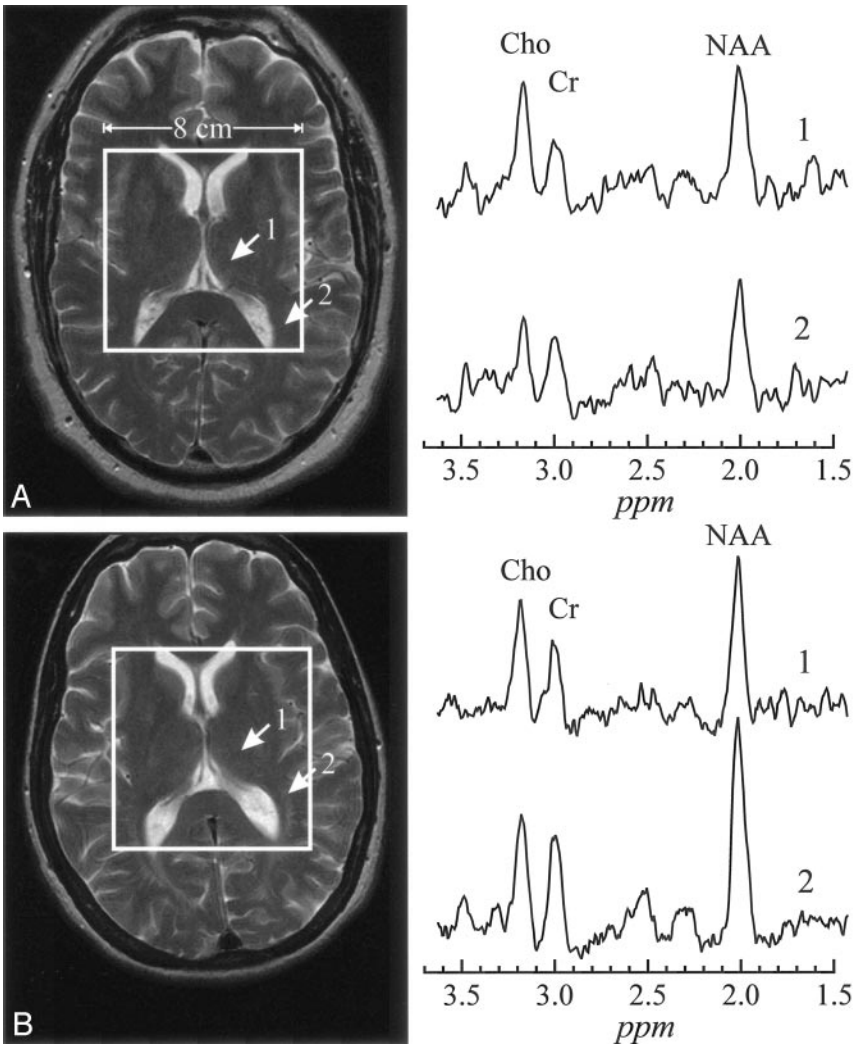

FIG 2. *A, top left*, T2-weighted image of a 54-year-old patient with late-onset $G_{M2}G$, superimposed with the 8 × 8 cm^2 ^{1}H-MR spectroscopy VOI. *Right,* Two spectra from thalamus and occipital white matter (*arrows* 1 and 2).

B, bottom left, Corresponding section from a matched control. The arrows indicate analogous regions to *A* for metabolite spectral comparisons. All spectra are on common intensity and chemical shift (parts per million) scales.

Note the characteristic lower NAA signal intensity in thalamus and NAWM in the patient (*A*) compared with the control (*B*), as well as decreased Cr and Cho.

TABLE 1: Demographics, clinical and genetic information for the patients with late-onset $G_{M2}G$

Patient No./ Age (y)/Sex	Disease Onset (Y)	Ambulation Index	Molecular Defect*
1/20/M	12	0	Exon 7, exon 11
2/32/M	15	2	Exon 7, R504C
3/28/M	13	3	Exon 7, exon 13
4/52/M	12	9	Exon 7, intron 12
5/29/F	17	4	Exon 7, exon 11
6/54/M	36	4	Exon 7, exon 11
7/31/F	12	2	Exon 7, exon 11
8/50/F	12	9	Exon 7, exon 11
9/58/M	17	7	Exon 7, exon 11

* Mutations: The exon 7 mutation involves a G to A transition at position 269 (G269S), which represents the most common disease allele associated with late-onset $G_{M2}G$. The exon 11 mutation (TATC1278) represents a frameshift mutation resulting from a 4-base insertion; this allele is the most frequent gene defect found either in homozygosity or heterozygosity among patients with the classic infantile form of Tay-Sachs disease.

of interest (VOI) was positioned in a central cerebellar region, as shown in Fig 1*A* VOI: 8-cm AP × 8-cm LR × 1.5-cm CC VOI, was positioned on the inferior border of the lateral ventricles to include part of the genu and splenium of the corpus callosum, the thalami, and the NAWM, as shown in Fig 2. Automated shimming yielded consistent 3.0 ± 0.3 Hz voxel line widths in all VOIs.

Our postprocessing software removed residual water and broad signals from the MR spectroscopy data in the time domain (22, 23), apodized with a 3-Hz lorentzian, Fourier-transformed in the spectral and spatial directions, and automatically frequency 0- and 1st-order phase–corrected in reference to the NAA and Cho peaks in each voxel (24). The relative amounts of the NAA, Cr and Cho in every voxel of each subject were estimated from their spectral peak areas by using the parametric spectral modeling and least-squares optimization method of Soher et al (25). These relative quantities were converted into absolute concentrations against the signal intensity from a 3-L sphere of 0.033 mol of NAA in water (18). In this quantification process, we took into account the differences in relaxation longitudinal, T_1, and transverse, T_2, relaxation times between the phantom in vitro (NAA only, $T1^{vitro}$ = 1.4 seconds, $T2^{vitro} \approx 0.5$ seconds) and those reported in vivo by using (18)

$$S_{corrected} \approx S(vitro) \cdot \left(1 - \frac{TE \cdot (T_2^{vivo} - T_2^{vitro})}{T_2^{vivo} \cdot T_2^{vitro}}\right) \cdot \frac{T_1^{vitro}}{T_1^{vivo}}$$

for NAA, Cho or Cr

Using the in vivo T1/T2 values reported in the literature, NAA = 1.4/0.43 seconds; Cr = 1.6/0.21 seconds; and Cho = 1.2/0.36 seconds (26, 27). Possible regional T1 or T2 variations

TABLE 2: ^{1}H-MR spectroscopy findings in patients with late-onset $G_{M2}G$

	Thalamus			White Matter			Cerebellum		
Patient	NAA	Cr	Cho	NAA	Cr	Cho	NAA	Cr	Cho
1	6.16	3.35	1.06	4.47	2.49	0.75	4.25	3.65	1.30
2	6.35	3.72	1.26	5.38	3.69	1.14	3.77	1.54	0.66
3	6.20	3.09	0.95	4.75	2.49	0.81	5.54	2.14	0.78
4	7.73	4.20	1.16	7.76	4.81	1.01	N/A	N/A	N/A
5	10.13	5.36	1.45	8.67	6.17	1.93	6.35	4.96	1.93
6	8.10	4.37	1.43	8.76	5.31	1.89	9.38	7.06	2.45
7	4.58	2.69	0.71	3.43	2.14	0.57	2.57	1.30	0.43
8	5.40	3.93	0.74	5.25	3.58	0.47	1.33	1.27	0.52
9	3.77	2.56	0.71	3.29	2.65	0.69	1.37	0.92	0.32
Patients 1–9	**6.50 ± 1.9**	3.69 ± 0.8	1.03 ± 0.3	**5.75 ± 2.1**	3.70 ± 1.4	1.05 ± 0.5	4.3 ± 2.7	**2.9 ± 2.2**	1.05 ± 0.8
Controls (n = 8)	11.0 ± 2.7	5.43 ± 1.2	1.43 ± 0.4	9.92 ± 2.7	5.20 ± 1.6	1.40 ± 0.4	11.1 ± 1.1	8.7 ± 1.3	2.4 ± 0.3

Concentrations of the 3 metabolites are in millimolars. Bold entries (for patients) are significantly different from the controls (P = .005).

were ignored, because similar anatomies were compared among all subjects. For quantification purposes in the cerebellum, because of the marked atrophy, we selected a voxel in the central white matter of the left hemisphere to include as much remaining tissue as possible. In the supratentorial brain, we selected a voxel in the center of the left thalamus and a voxel in the occipital white matter laterally to the occipital horn of the lateral ventricle.

Statistical Analyses

Nonparametric Kruskal-Wallis test of variance was used to compare MR spectroscopy data between patients and controls. Absolute levels of NAA, Cr, and Cho from the patients were correlated with their ambulation index and age at disease onset by using the nonparametric Spearman test. Results were declared significant at the 5% level (ie, $P \leq .05$).

Results

Cerebellum

All late-onset $G_{M2}G$ patients exhibited the radiologic hallmark of severe cerebellar atrophy, as shown in Fig 1. ^{1}H-MR spectroscopy was obtained from 8/9 patients. Cerebellar metabolites levels, not corrected for CSF fraction in the voxels, are compiled in Table 2. Although all metabolites were 20%–90% lower than those of controls, only NAA (4.3 ± 2.7 vs 11.1 ± 1.1 mmol/L [mean ± SD] and Cr (2.9 ± 2.2 vs 8.7 ± 1.3 mmol/L) were significantly different (P = .02 in both cases), whereas Cho (1.1 ± 0.9 vs 2.4 ± 0.3 mmol/L) did not reach the level of statistical significance (P = .07).

Supratentorial Brain

None of the patients exhibited any supratentorial MR imaging abnormalities, as shown in Fig 2. The ^{1}H-MR spectroscopy results reported in Table 2, nevertheless, show significantly decreased NAA levels in the patients compared with the controls' average in both the thalamus (6.49 ± 1.9 vs 11.0 ± 2.7 mmol/L [P = .003]) and the NAWM (5.75 ± 2.1 vs 9.92 ± 2.7 mmol/L [P = .005]). Patients' thalamic Cr = 3.69 ± 0.8 versus 5.43 ± 1.2 mmol/L and Cho = 1.05 ± 0.3 versus 1.43 ± 0.4 mmol/L, as well as NAWM Cr = 3.70 ± 1.4 versus 5.20 ± 1.6 mmol/L and Cho = 1.03 ± 0.5 versus 1.40 ± 0.4 mmol/L, levels were also lower than controls', but neither difference reached the level of statistical significance. No relationships were found between cerebral metabolite levels and ambulation index (AI) or age at disease onset.

Discussion

To the best of our knowledge, this is the first time that brain metabolism of late-onset $G_{M2}G$ has been investigated by using ^{1}H-MR spectroscopy. The current study showed a diffuse pattern of neuronal/axonal involvement in these patients both infra- and supratentorial brain structures with and without MR imaging visible changes, respectively.

Because the most striking radiologic feature in this disease is cerebellar atrophy, we extracted and compared one voxel from the 2D array in each of the patients and the controls, as shown in Fig 1. Because we could not segment the CSF fraction in these voxels, we can only reason that, if it were partial CSF volume contamination, the same percentage level losses for all 3 metabolites should be seen. In the cerebellum of 4/8 patients, however—patients 1, 3, 5, and 6 in Table 1—the disproportionate loss of NAA and Cr compared with Cho could not be explained by such partial volume alone. Therefore, it probably reflects a greater neuronal loss in the remaining tissue. In the other 5 patients, proportional decline of all 3 metabolites reflects CSF partial volume (in contrast to Fig 1) from severe atrophy, which exceeded 75%. Such substantial tissue loss may make differential level change detection difficult by being at or below the sensitivity of the method. For example, looking for 15% change in the remaining 25% of cerebellar tissue in a voxel requires ~3.5% sensitivity, below the ±5%–10% reported for ^{1}H-MR spectroscopy (28). Because in $G_{M2}G$ demyelination is secondary to neuronal cell injury, this relatively lower Cho loss finding is in line with the known pathogenesis of this disease.

Supratentorial regions of these patients exhibited a diffuse pattern of neuronal/axonal involvement, reflected by a significant (~40%) reduction of NAA in

both the thalamus and occipital white matter, which were otherwise both unremarkable on MR imaging. Because the late-onset form of the disease is milder and the patients survive longer after diagnosis, only very few cases have been studied postmortem (5, 10, 29–32). Nevertheless, the neuropathologic features have consistently shown marked loss of both Purkinje and granul cells in the cerebellum, as well as widespread neuronal G_{M2} storage throughout the neuroaxis, which is usually more pronounced in the deep nuclear structures, thalamus, brain stem, and spinal anterior horn cells than in the cerebral cortex (5, 10, 29–32). These swollen storage neurons contain characteristic periodic acid-Schiff–positive G_{M2} inclusions, which are generally known as membranous cytoplasmic bodies (MCB). The progression of this neuronal G_{M2} storage leads to perikaryal enlargement, ectopic dendritogenesis, and the expansion of axon hillocks (meganeurites) (10). It has been speculated that (1) neuronal storage leads directly to cell death, because metabolites of the storage lipid are toxic to neurons, and (2) the abnormal ectopic dendrites and morphologic changes in storage neurons affect their function (33).

Although NAA is widely considered to be a marker of neuronal loss or degeneration, experimental and clinical studies suggest that it could also be a marker of damage. Its decrease, therefore, could also be due to subclinical metabolic neuronal dysfunction rather than loss (34, 35). These 2 pathologic processes (dysfunction and loss), however, are not mutually exclusive. Although the pathogenetic mechanism detrimental to neurons is largely unknown, it is likely that cell loss in supratentorial structures is milder and slower than in the cerebellum. Therefore, neuronal loss might be masked by the swelling of surviving neurons and by the proliferation of ectopic dendrites, thus resulting in the absence of macroscopic MR imaging–visible atrophy. The decrease of Cr (~30%) and Cho (~26%) in our patients seems to support the hypothesis of neuronal loss in addition to dysfunction. Because neurons also contain Cr and Cho, neuronal loss would be expected to lead to a decline in those 2 metabolites in addition to the decrease in NAA. Furthermore, the presence of MCBs in astrocytes (33) suggests that glial cells might be involved in the same pathologic process contributing to Cr and Cho decrease. The decrease of Cho is in line with the results of a recent study with ^{31}phosphorus (^{31}P) MR spectroscopy, which reported a decrease of phosphodiesters and membrane-bound phosphates in a patient with late-onset $G_{M2}G$ (36). Unlike our patients, the level of Cr was normal in their case. Because only phosphocreatine is detectable on the ^{31}P spectrum, whereas the Cr peak of a proton spectrum comprises creatine plus phosphocreatine, we believe that the decrease of Cr in our patients is likely to be due to a decrease of creatine rather than phosphocreatine.

The metabolic decline in NAWM is not surprising if we consider that neurons and myelin sheaths are interdependent; loss of one will eventually lead to the destruction of the other. Therefore, axons of neurons undergoing ganglioside storage will not be spared, and focal swellings, "spheroids," or neuroaxonal dystrophy will eventually lead to Wallerian degeneration (37). Furthermore, because 70% of the myelin dry weight consists of lipids (38) and because sequestering of G_{M2} gangliosides is accompanied by secondary trapping of other substrates, including phospholipids and cholesterol (37), the decrease of Cho in our patients might also reflect abnormalities in the myelin structure.

The lack of correlation between the metabolite levels and the AI is not entirely unexpected. First, the cohort was small, and the AI was the only clinical rating score available. It is of interest, however, that patients 5 and 6, whose MR imaging findings were relatively normal, presented very mild neurologic dysfunctions. Second, our spatial resolution and 2D coverage precluded probing more potentially informative anatomic structures, possibly limiting the strength of our clinical-metabolic correlations. Finally, the heterogeneity of causal mutation may have contributed to the lack of relationship between age of onset and disease severity as assessed by the functional ambulatory test. Nevertheless, our study suggests that in late-onset $G_{M2}G$ neuronal/axonal injury is both diffuse and widespread, with changes detectable beyond the MR imaging-visible cerebellar atrophy. This might partially explain the recent findings of risk of impairment in executive functioning and memory in late-onset $G_{M2}G$ patients (6). Although cognitive deficits were partially attributed to cerebellar atrophy, no relationship was found between this finding and the degree of cerebellar dysfunction.

The ability of ^{1}H-MR spectroscopy to detect abnormalities that precede MR imaging changes also has a practical implication: to quantify objectively the extent of neuroaxonal degeneration in patients with signs of neurologic deterioration and supratentorial normal MR imaging. An early diagnosis for this disease is particularly important, because preclinical studies in a mouse model of Tay-Sachs disease has shown that substrate reduction therapy prevents ganglioside storage in the CNS, reducing neurologic deficits and slowing disease progression (39, 40). Because of residual catabolic enzyme activity, patients with late-onset $G_{M2}G$ are the best candidates to receive substrate reduction therapy, and therefore the NAA level might represent a useful surrogate marker to monitor responses to the treatment.

Conclusion

^{1}H-MR spectroscopy is both sensitive and specific to neuroaxonal damage in late-onset $G_{M2}G$ patients, even in the absence of radiologic abnormalities on conventional MR imaging. Because ganglioside accumulation can be reduced by pharmacologic agents, ^{1}H-MR spectroscopy might indeed be a sensitive and specific technique for detecting and quantifying the neuroaxonal injury status and monitoring the response to current and emerging treatments. Therefore, more extensive MR spectroscopy studies to ex-

plore larger brain regions, including subcortical frontal white matter and cortical gray matter, are necessary to elucidate the metabolic correlates of neurologic and cognitive deficits in $G_{M2}G$ patients.

References

1. Navon R, Argov Z, Frisch A. **Hexosaminidase A deficiency in adults.** *Am J Med Genet* 1986;24:179–196
2. Walkley SU. **Neurobiology and cellular pathogenesis of glycolipid storage diseases.** *Philos Trans R Soc Lond B Biol Sci* 2003;358:893–904
3. Navon R. **Late-onset GM2 gangliosidosis and other hexosaminidase mutations among Jews.** *Adv Genet* 2001;185–197
4. Argov Z, Navon R. **Clinical and genetic variations in the syndrome of adult GM2 gangliosidosis resulting from hexosaminidase A deficiency.** *Ann Neurol* 1984;16:14–20
5. Brett EM, Ellis RB, Haas L, et al. **Late onset GM2-gangliosidosis: clinical, pathological, and biochemical studies on 8 patients.** *Arch Dis Child* 1973;48:775–785
6. Zaroff CM, Neudorfer O, Morrison C, et al. **Neuropsychological assessment of patients with late onset GM2 gangliosidosis.** *Neurology* 2004;62:2283–2286
7. Fukumizu M, Yoshikawa H, Takashima S, et al. **Tay-Sachs disease: progression of changes on neuroimaging in four cases.** *Neuroradiology* 1992;483–486
8. Streifler JY, Gornish M, Hadar H, Gadoth N. **Brain imaging in late-onset GM2 gangliosidosis.** *Neurology* 1993;43:2055–2058
9. Mugikura S, Takahashi S, Higano S, et al. **MR findings in Tay-Sachs disease.** *J Comput Assist Tomogr* 1996;20:551–555
10. Suzuki K. **Neuropathology of late onset gangliosidoses: a review.** *Dev Neurosci* 1991;205–210
11. Ross B, Bluml S. **Magnetic resonance spectroscopy of the human brain.** *Anat Rec* 2001;265:54–84
12. Tedeschi G, Schiffmann R, Barton NW, et al. **Proton magnetic resonance spectroscopic imaging in childhood ataxia with diffuse central nervous system hypomyelination.** *Neurology* 1995;45:1526–1532
13. Tedeschi G, Bonavita S, Barton NW, et al. **Proton magnetic resonance spectroscopic imaging in the clinical evaluation of patients with Niemann-Pick type C disease.** *J Neurol Neurosurg Psychiatry* 1998;65:72–79
14. Tedeschi G, Bonavita S, Banerjee TK, et al. **Diffuse central neuronal involvement in Fabry disease: a proton MRS imaging study.** *Neurology* 1999;52:1663–1667
15. Tedeschi G, Bertolino A, Lundbom N, et al. **Cortical and subcortical chemical pathology in Alzheimer's disease as assessed by multislice proton magnetic resonance spectroscopic imaging.** *Neurology* 1996;47:696–704
16. Fu L, Matthews PM, De Stefano N, et al. **Imaging axonal damage of normal-appearing white matter in multiple sclerosis.** *Brain* 1998;121:103–113
17. De Stefano N, Narayanan S, Matthews PM, et al. **In vivo evidence for axonal dysfunction remote from focal cerebral demyelination of the type seen in multiple sclerosis.** *Brain* 1999;122:1933–1939
18. Inglese M, Li BS, Rusinek H, et al. **Diffusely elevated cerebral choline and creatine in relapsing-remitting multiple sclerosis.** *Magn Reson Med* 2003;50:190–195
19. Inglese M, Ge Y, Filippi M, et al. **Indirect evidence for early widespread gray matter involvement in relapsing-remitting multiple sclerosis.** *Neuroimage* 2004;21:1825–1829
20. Patel SH, Inglese M, Glosser G, et al. **Whole-brain N-acetylaspartate level and cognitive performance in HIV infection.** *AJNR Am J Neuroradiol* 2003;24:1587–1591
21. Miller BL. **A review of chemical issues in 1H NMR spectroscopy: N-acetyl-L-aspartate, creatine and choline.** *NMR Biomed* 1991;4:47–52
22. Marion D, Ikura M, Bax A. **Improved solvent suppression in one- and two-dimensional NMR spectra by convolution of time domain data.** *J Magn Reson* 1989;84:425–430
23. Campbell ID, Dobson CM, Williams RJP, Xavier ZV. **Resolution enhancement of protein PMR spectra using the difference between a broadened and normal spectrum.** *J Magn Reson* 1973;11:172–181
24. Gonen O, Murdoch JB, Stoyanova R, Goelman G. **3D multivoxel proton spectroscopy of human brain using a hybrid of 8th-order Hadamard encoding with 2D chemical shift imaging.** *Magn Reson Med* 1998;39:34–40
25. Soher BJ, Young K, Govindaraju V, Maudsley AA. **Automated spectral analysis. III. Application to in vivo proton MR spectroscopy and spectroscopic imaging.** *Magn Reson Med* 1998;40:822–831
26. Barker PB, Soher BJ, Blackband SJ, et al. **Quantitation of proton NMR spectra of the human brain using tissue water as an internal concentration reference.** *NMR Biomed* 1993;6:89–94
27. Kreis R, Ernst T, Ross B. **Absolute concentrations of water and metabolites in the human brain. II. Metabolite concentrations.** *J Magn Reson* 1993;102:9–19
28. Li BS, Babb JS, Soher BJ, et al. **Reproducibility of 3D proton spectroscopy in the human brain.** *Magn Reson Med* 2002;47:439–446
29. Suzuki K, Rapin I, Suzuki Y, Ishii N. **Juvenile GM2-gangliosidosis: clinical variant of Tay-Sachs disease or a new disease.** *Neurology* 1970;20:190–204
30. Menkes JH, O'Brien JS, Okada S, et al. **Juvenile GM2 gangliosidosis: biochemical and ultrastructural studies on a new variant of Tay-Sachs disease.** *Arch Neurol* 1971;25:14–22
31. Buxton P, Cumings JN, Ellis RB, et al. **A case of GM2 gangliosidosis of late onset.** *J Neurol Neurosurg Psychiatry* 1972; 35:685–692
32. Rapin I, Suzuki K, Valsamis MP. **Adult (chronic) GM2 gangliosidosis: atypical spinocerebellar degeneration in a Jewish sibship.** *Arch Neurol* 1976;33:120–130
33. Jeyakumar M, Butters TD, Dwek RA, Platt FM. **Glycosphingolipid lysosomal storage diseases: therapy and pathogenesis.** *Neuropathol Appl Neurobiol* 2002;28:343–357
34. Brenner RE, Munro PM, Williams SC, et al. **The proton NMR spectrum in acute EAE: the significance of the change in the Cho: Cr ratio.** *Magn Reson Med* 1993;29:737–745
35. De Stefano N, Matthews PM, Antel JP, et al. **Chemical pathology of acute demyelinating lesions and its correlation with disability.** *Ann Neurol* 1995;38:901–909
36. Felderhoff-Mueser U, Sperner J, Konstanzcak P, et al. **31Phosphorus magnetic resonance spectroscopy in late-onset Tay-Sachs disease.** *J Child Neurol* 2001;16:377–380
37. Walkley SU. **Secondary accumulation of gangliosides in lysosomal storage disorders.** *Semin Cell Dev Biol* 2004;15:433–444
38. Coetzee T, Suzuki K, Popko B. **New perspectives on the function of myelin galactolipids.** *Trends Neurosci* 1998;21:126–130
39. Platt FM, Neises GR, Reinkensmeier G, et al. **Prevention of lysosomal storage in Tay-Sachs mice treated with N-butyldeoxynojirimycin.** *Science* 1997;276:428–431
40. Butters TD, Dwek RA, Platt FM. **Therapeutic applications of imino sugars in lysosomal storage disorders.** *Adv Exp Med Biol* 2003;561–574